

An Indirect Measurement of ${}^6\text{Li}(n,\gamma)$ Cross Sections

Midhun C.V^{1,*}, M.M Musthafa^{1,†}, S.V Suryanarayana^{2,3}, Gokuldas H¹, Shaima A¹, Hajara. K¹, Antony Joseph¹, T. Santhosh², A. Baishya², A Pal², P.C Rout², S Santra², P.T.M Shan¹, Satheesh B⁴, B. V. John², K.C Jagadeesan⁵, and S. Ganesan⁶

¹ Dept. of Physics, University of Calicut, Calicut University P.O Kerala, 673635 India

² Nuclear Physics Division, Bhabha Atomic Research Centre, Mumbai 400085, India

³ Manipal Centre for Natural Sciences, MAHE, Manipal - 576014, India

⁴ Dept. of Physics, Mahatma Gandhi Government Arts College, Mahe, 673311, India

⁵ Radiopharmaceuticals Division, Bhabha Atomic Research Centre, Mumbai 400085, India and

⁶ Formerly Raja Ramanna Fellow, Bhabha Atomic Research Centre, Mumbai 400085, India

(Dated: September 27, 2022)

The ${}^6\text{Li}(n,\gamma){}^7\text{Li}$ cross sections in the neutron energy range of 0.6 to 4 MeV have been measured by the experimental implementation of the direct capture formalism. This was done by measuring the γ transition probability experimentally and accounting for the spin factor by theoretical calculation. The electromagnetic transition probabilities from ${}^7\text{Li}^*$ analogous to the initial neutron capture states of ${}^6\text{Li}+n$ were measured by populating the J_i states of ${}^7\text{Li}$ through ${}^7\text{Li}(p,p'){}^7\text{Li}^*$ reaction. The impact of coupling of resonant states, above neutron separation threshold of ${}^7\text{Li}$, in the neutron capture, is observed from the capture γ spectrum. The measured cross sections were reproduced through FRESKO and Talys-1.95 Direct Capture Calculations.

Neutron induced reactions on Li isotopes are having a renewed interest due to their involvement in nuclear astrophysics and Gen.IV nuclear reactors[1–3]. Though ${}^6\text{Li}(n,\gamma)$ reaction is having a significant importance, the reaction remains thus far unexplored. As the abundance ratio of ${}^6\text{Li}$ to ${}^7\text{Li}$ is used as an observable for estimating the time scale of stellar evolution, the reaction is having a major role in the Standard Big Bang Nucleosynthesis (SBBN) network calculations[1, 4, 5]. Further, ${}^6\text{Li}(n,t)$ and ${}^6\text{Li}(n,n't)$ reaction contribute to the ${}^3\text{H}$ breeding in fusion reactors [6]. In the emergency shut down system of fast neutron reactors, lithium enriched in ${}^6\text{Li}$ is used. In these cases, ${}^6\text{Li}(n,\gamma)$ reaction also will be initiated due to the high flux neutron environment and remains as the major source of uncertainty in the tritium production[7].

The abundances of ${}^6\text{Li}$ and ${}^7\text{Li}$ are highly influenced by the ${}^6\text{Li}(n,\gamma)$ reaction rates. In order to avoid the wrong estimations and biasing in the SBBN network calculations, the cross section for this channel has to be accurately measured[1, 4, 5]. However, the ${}^6\text{Li}(n,\gamma)$ reaction remains not well explored due to its small cross section as well as the lesser natural abundance of ${}^6\text{Li}$. The ${}^6\text{Li}(n,\gamma){}^7\text{Li}$ exhibits considerably small cross sections, in the order of μb , due to the predominance of $\alpha + t$ breakup mode, ${}^6\text{Li}(n,\alpha){}^3\text{H}$ channel being prominent. This breakup mode having a threshold of 2.47 MeV, dominates as the Q-value for the neutron capture of ${}^6\text{Li}$ is as high as 7.25 MeV. Due to this higher Q-value, breakup levels populate more than the single particle levels. This suppresses the radiative neutron capture process in ${}^6\text{Li}$. However, the direct reaction component involving the single particle levels contributes significantly

to the radiative neutron capture through Direct Capture (DC) mechanism [8, 9].

There is only a single measurement on energy dependant cross section of ${}^6\text{Li}(n,\gamma)$ existing in the literature, by Ohsaki et al., for the neutron energy range of 20 to 80 keV[10]. The other measurements available as exfor entries [11], by R. B Firestone et al. [12], Chang Su Park et al. [13] and G.A Batholomew et al. [14] are the Maxwellian averaged cross sections for thermal reactor neutron spectrum. Further, there are evaluations existing for ${}^6\text{Li}(n,\gamma)$ in ENDF/B-VIII.0 [15], JEEF [16] and JENDL[17] basic evaluated nuclear data libraries. They are the derived data sets estimated by fitting the R-Matrix formalism on ${}^6\text{Li}(n,t){}^4\text{He}$ cross sections[15]. Due to the limitations with the ${}^6\text{Li}$ target and lower cross sections, the direct measurement of ${}^6\text{Li}(n,\gamma)$ is potentially challenging.

As a solution to this problem, an experimental methodology has been implemented by utilizing the properties of the Direct Capture formalism. The measurement of ${}^6\text{Li}(n,\gamma)$ cross sections has been attempted through this method, by populating the initial neutron capture states by inelastic scattering of protons on ${}^7\text{Li}$. The γ transitions from the ${}^7\text{Li}$ initial state to bound states of ${}^7\text{Li}$ are measured by generating $p - \gamma$ coincidences. The capture cross sections were determined through the approach of Direct Capture mechanism, reformulated for the experimental implementation. The current experiment is having resemblances with the established Oslo method[18, 19]. In this study, only a single large volume LaBr_3 scintillator was used instead of γ calorimeter. This measurement has been successful because all the γ events from the initial neutron capture states are well resolvable and γ multiplicity is near to unity.

The direct capture model (DC) is well established for explaining the radiative captures at lower energies, and

* midhun.chemana@gmail.com

† mmm@uoc.ac.in

neutron capture reactions for light elements, where the compound nuclear level density models are insufficient to explain the radiative capture[9]. The DC accounts for the capture cross section as the sum of direct capture to the discrete states and the single particle continuum states. The Direct Capture formalism is expressed in its own form based on Ref. [8] and Ref. [9],

$$\sigma^{DC}(E) = \sum_{f=0}^{f_{max}} S_f \sigma_f^{dis}(E) + \langle S \rangle \int_{E_0}^{E_n} \rho(E_f, J_f, \pi_f) \sigma_f^{con}(E_f) dE_f \quad (1)$$

The first part in Eq. 1, $\sum_{f=0}^{f_{max}} S_f \sigma_f^{dis}(E_f)$ corresponds to the direct capture to the discrete resonant states defined as f . S_f is the spectroscopic amplitude corresponding to each resonant state. Second part, $\langle S \rangle \int_{E_0}^{E_n} \rho(E_f, J_f, \pi_f) \sigma_f^{con}(E_f) dE_f$ corresponds to the capture to the single particle continuum states. The $\langle S \rangle$ is the average spectroscopic amplitude of the continuum states distributed from the continuum formation threshold E_0 to the neutron separation energy E_n . $\rho(E_f, J_f, \pi_f)$ is the single particle level densities corresponding to each E_f , which are also a function of the spin and parity of the state. The $\sigma_f^{con}(E_f)$ stands for the capture corresponding to the each of f states in the continuum having energy E , which is assumed to be discretized in an interval dE_f . The $\sigma_f^{con}(E_f)$ can be expressed, based on the electric and magnetic modes of transition, as

$$\sigma_f^{con}(E_f) = \frac{2J_f + 1}{Ek(2J_A + 1)(2J_n + 1)} \times \sum_{I_f, J_i, l_i, I_i} [C_1 k_\gamma^3 (|M_{E1}|^2 + |M_{M1}|^2) + C_2 k_\gamma^5 |M_{E2}|^2] \quad (2)$$

Here J_f is the spin of the final state after capture followed by the electromagnetic transition, J_A is the spin of the target nuclei and J_n is the spin of neutron. E and k are respectively energy and wave number of neutrons corresponding to J_i . C_1 and C_2 are the normalization constants corresponding to dipole and quadrupole transitions. M_{E1} , M_{M1} are the electric and magnetic dipole matrix elements and M_{E2} is the matrix element corresponding to electric quadrupole transition. k_γ stands for the wave number of the emitted photon.

The neutron capture in ${}^6\text{Li}$ populates initial capture state with an excitation energy of $7.25 \text{ MeV} + E_n(\frac{A}{A+1})$. This energy is well above the ${}^7\text{Li} \rightarrow \alpha + t$ breakup threshold of 2.47 MeV . However, the transition from J_i to the $\alpha + t$ breakup continuum levels will not contribute to the radiative capture process. The population of breakup states results to the continuum breakup of ${}^7\text{Li}$. Hence, the $3/2^-$ and $1/2^-$ states corresponding to ground and 477 keV are the only J_f states involving the radiative capture. The present formulation assumes that the $3/2^-$ and $1/2^-$ states are also a part of the single particle continuum states. However, for these states, the $\rho(E_f, J_f, \pi_f)$ term generates the definite shape of the resonance. This

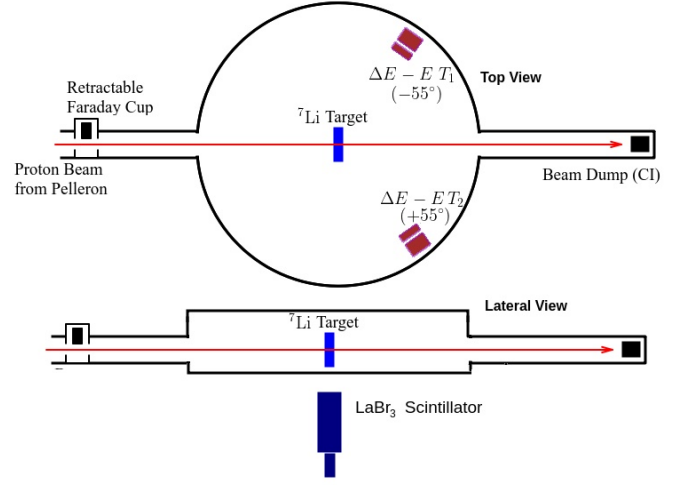


FIG. 1. Illustration of experimental setup in top and lateral views

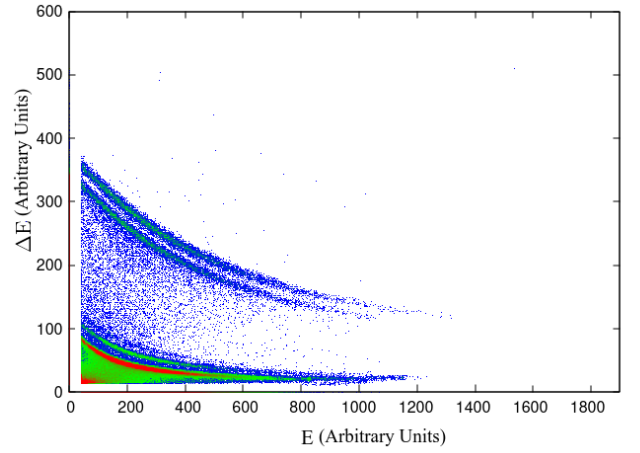


FIG. 2. The typical $E - \Delta E$ Correlation plot recorded in the telescope

assumption is taken for modifying Eqn. 1 to a single integral ranging from 0 to E_n . Hence the reformulated form can be expressed as,

$$\sigma^{DC}(E) = \frac{(2J_f + 1)}{Ek(2J_A + 1)(2J_n + 1)} \int_0^{E_n} \rho(E_f, J_f, \pi_f) \times \sum C_1 k_\gamma^3 (|M_{E1}|^2 + |M_{M1}|^2) + C_2 k_\gamma^5 |M_{E2}|^2 dE_f \quad (3)$$

In the following part of the article, $\frac{(2J_f+1)}{Ek(2J_A+1)(2J_n+1)}$ is expressed as g_j , the spin factor, and $\int_{E_x}^{E_{max}} \rho(E_f, J_f, \pi_f) \times \sum C_1 k_\gamma^3 (|M_{E1}|^2 + |M_{M1}|^2) + C_2 k_\gamma^5 |M_{E2}|^2 dE_f$ as $\Gamma(E_x)$, gamma strength term.

The gamma rays produced from each excitation energy, equivalent to the excitation energy of the neutron capture, having a capture γ distribution depend on the transitions to J_f states. The integral of this distribution is considered as $\Gamma(E_x)$, which has been measured in the

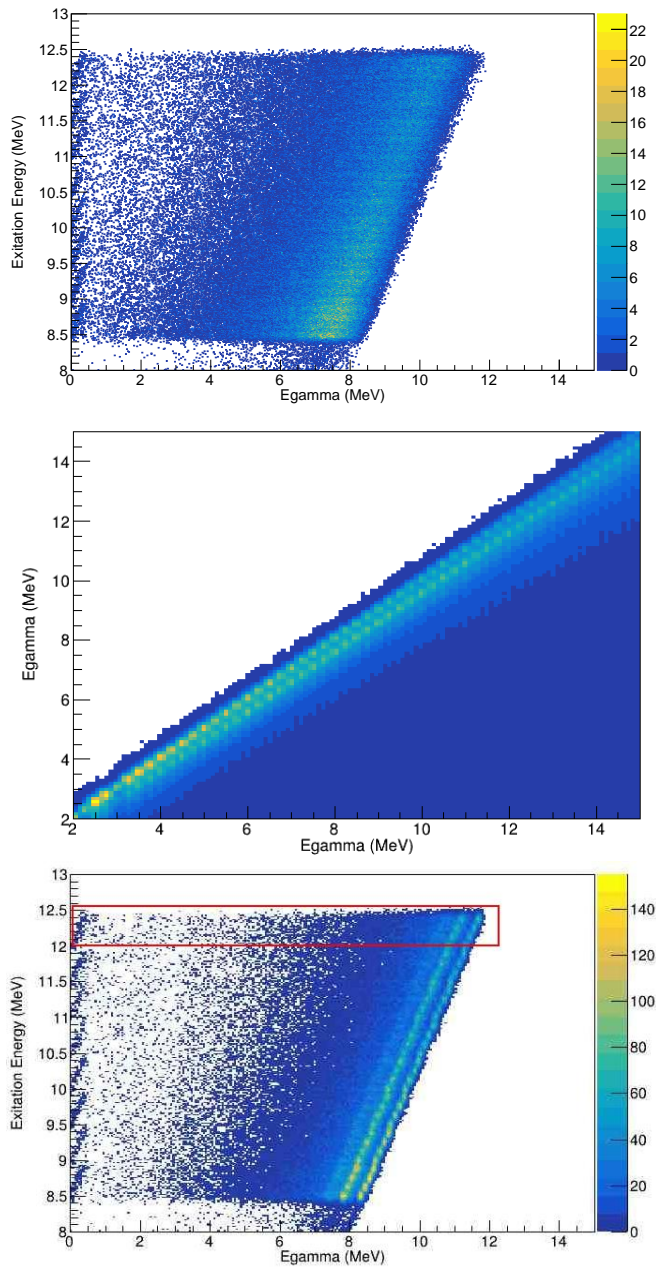


FIG. 3. (a): The original E_γ - E_x correlation, (b) : The response matrix for LaBr₃ scintillation detector, (c): The unfolded E_γ - E_x correlation matrix with the gate defined for 12.375 MeV excitation

current experiment. The events populating resonant and direct breakup levels, during the collective excitation, are not producing any gamma rays. Thus the γ spectra produced in inelastic excitation of ${}^7\text{Li}$ are purely from the transition of the J_i states to the bound states. Thus in the current study, $\Gamma(E_x)$ is measured for the equivalent neutron energies using inelastic scattering of protons on Li target. The g_i has been calculated theoretically for obtaining the cross sections.

The experiment is performed using 16 MeV proton beam from BARC-TIFR Pelletron facility, Mumbai, India. A ${}^{nat}\text{Li}$ target of 1.4 mg/cm² was used for the experiment. The experimental setup has been illustrated in Fig 1. Two silicon detector telescopes having 25 μm and 1500 μm ΔE - E pairs, were mounted at $+55^\circ$ -55° at a distance of 7.5cm from the target to record the inelastically scattered protons. A 3' diameter and 7' length LaBr₃ scintillator, coupled to a fast photomultiplier tube, was placed at 90° , at the bottom side of the target. This was used for measuring the γ spectra. The distance between the target and LaBr₃ detector was 12 cm.

The inelastically scattered protons were identified from the E - ΔE correlation plot by proper gating. The γ events in the LaBr₃ scintillator, with the elastically scattered protons are identified. The events were converted to the excitation energy of ${}^7\text{Li}$ from the energy of elastically scattered protons, using two body kinematics. A correlation matrix between γ energy (E_γ) and excitation energy of ${}^7\text{Li}$ (E_x) was constructed. This matrix was unfolded to original γ matrix using response matrix for the current LaBr₃ detector. The unfolding procedure was done using in-house developed machine learning assisted unfolding algorithm by preserving the excitation energy information of the events[20]. The obtained E - ΔE correlation plot is presented in Figure. 2. The measured correlation, simulated response matrix for the detector and unfolded E_γ - E_x matrix are shown in Figure. 3.

The unfolded γ matrix has been appropriately gated for the excitation energy and projected to the γ spectrum. The spectrum holds three colonies of gammas, evident in all excitation energies. Discrete γ colonies are corresponding to the electromagnetic transitions from J_i state with energy E_x to the $3/2^-(g.s)$, $1/2^-(477\text{keV})$ states below $\alpha + t$ breakup threshold. The continuum γ colony is identified as emerging due to the coupling of $7/2^-, 5/2^-$ and $3/2^-$ resonant levels, above neutron separation threshold of ${}^7\text{Li}$, to the electromagnetic transitions to the $3/2^-(g.s)$ or $1/2^-(477\text{keV})$ states. These states are also overlapped by the $\alpha + t$ breakup continuum, results a higher decay width. The inelastic scattering populates the collective levels than the single particle levels in nuclei. In the case of ${}^7\text{Li}$, there are $\alpha + t$ breakup continuum present in the region of the collective levels. The population of the breakup levels seldom contributes to the γ production, as they end up with the breakup (the inelastic breakups). Hence the γ events observed in coincidence with the inelastically scattered protons can be assured as originated from the single particle levels.

The total counts in the γ colonies are retrieved and normalized with the inelastically scattered protons corresponding to the each excitation energy bin. The normalized γ yield is corrected for the solid angle between the LaBr₃ scintillator and the target. The attenuation in the bottom lid of the scattering chamber is also accounted based on Geant4 simulation [21]. The intrinsic efficiency of the detector has already been applied through the response matrix during the unfolding pro-

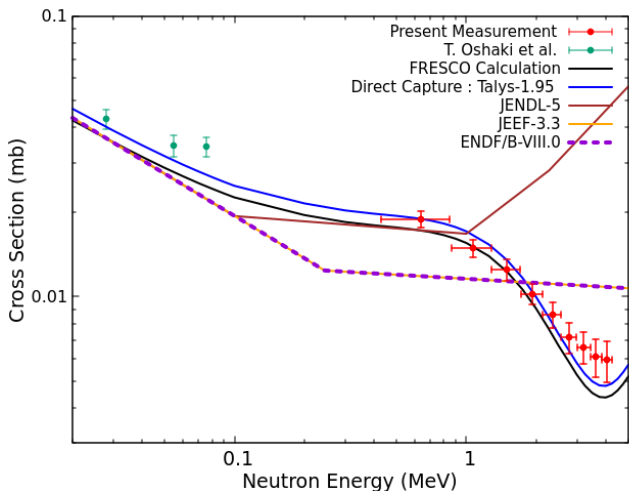


FIG. 4. Measured ${}^6\text{Li}(n, \gamma)$ cross sections compared with Direct Capture Model Calculations in FRESKO, Talys-1.95, and the evaluations by ENDF/B-VIII.0, JEEF-3.3 and JENDL-5 libraries

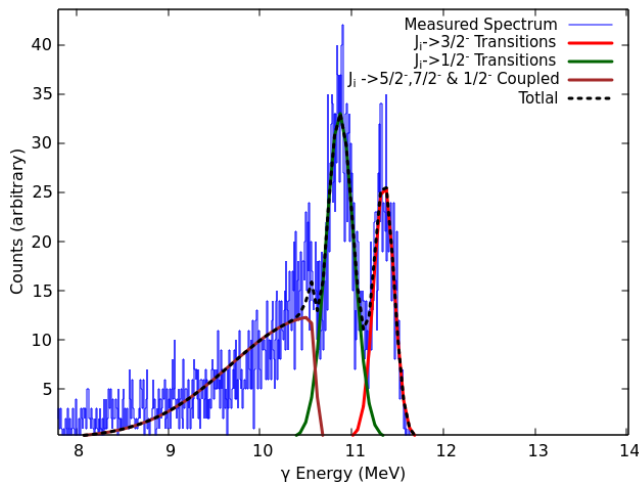


FIG. 5. Measured γ spectrum at 11.5 MeV excitation energy along with the calculated spectrum

cess. This corrected normalized yield is the measure of $\Gamma(E_x)$ in the Direct Capture Formalism. The spin factor, g_i , is calculated using the direct capture calculation module incorporated in Talys-1.95. This provides an accurate estimation of the wave number, k . Optical potential for $n+{}^6\text{Li}$ is taken from S. Chiba et al [22] for the calculation of the spin factor. The ${}^6\text{Li}(n, \gamma)$ cross sections were then deduced as $g_i\Gamma(E_\gamma)$.

Theoretical calculations are performed to reproduce the direct capture cross sections as well as to validate the measured γ spectrum. A coupled channel method has been adopted for the calculation. $n+{}^6\text{Li}$ is taken as the entrance channel mass partition and ${}^7\text{Li}+\gamma$ partition in the exit channel. The $n+{}^6\text{Li}$ potentials by Chiba et al.[22] was used for the calculations. The calculations

were performed using FRESKO coupled channel code [23]. The problem is defined as to calculate the direct radiative transitions from J_i to $3/2^- (g)$ and $1/2^- (477 \text{ keV})$ levels. The levels above neutron separation energy is considered as coupled to the $3/2^-$ and $1/2^-$ levels. Further, the overlap of $\alpha+t$ on the resonant states above the breakup threshold has been considered. The breakup continuum is discretized with $\alpha+t$ relative energy bin of 0.5 MeV, and the spin is calculated as the sum of spin of t and the relative angular momentum of the bin. Theoretical spectroscopic factor for ${}^6\text{Li}+n$ from the shell model calculations by Cohen and Kurath have been used for the resonant states[24]. An optimized average spectroscopic factor of 0.75 was used for $\alpha+t$. The FRESKO calculation has been limited to E_1 and M_1 mode of γ transitions and higher multiplicities have been neglected. A separate Monte-Carlo calculation, based on the FRESKO calculated cross sections, has been performed to reproduce the experimentally measured γ spectra.

Along with the FRESKO calculations, statistical Direct Capture calculations were performed using Talys-1.95 nuclear reaction code [25]. This is to account for the compound nuclear, pre-equilibrium and the continuum component of the direct capture mechanism. The Microscopic level densities (temperature dependent HFB, Gogny force) from Hilaire's combinatorial tables were used for the calculations of compound nuclear contribution as well as the continuum component of direct capture[26]. The predictions by Talys calculations were also compared with experimental results.

The measured cross sections for ${}^6\text{Li}(n, \gamma)$ are illustrated as locally averaged histogram values in Figure 4, along with the measurement by T. Oshaki et al., for comparison. Theoretical calculations using FRESKO and Talys-1.95 are also presented in Figure 4. Present measurement of cross sections for ${}^6\text{Li}(n, \gamma)$ is limited to the Direct Capture, and the compound nuclear contributions. Due to the limitations in the methodology, pre-equilibrium contribution is not addressed in the experiment. Measured cross sections are in the μb range and cover, for the first time, energies of 0.6 to 4 MeV as compared to measurements of Oshaki et al. which are in the range of 30 to 70 keV energy region.

The FRESKO calculated discrete component of the Direct Capture is illustrated as the black solid line in Figure. 4. The calculations reproduce the experimental cross sections within the error bars, for the spectroscopic factors by Kohan and Kurath. This indicates that the major contribution of the ${}^6\text{Li}(n, \gamma)$ is from the discrete component of the direct neutron capture. Further, there exists a strong coupling of $5/2^-$, $7/2^-$ and $3/2^-$ levels, which lies above the neutron separation threshold of ${}^7\text{Li}$, on $J_i \rightarrow 3/2^-$ and $J_i \rightarrow 1/2^-$ transitions. These resonant states are overlapping with the $\alpha+t$ breakup continuum and indicates a larger energy width. This coupling effect is emerged as the low energy tail along with γ colonies, corresponding to $J_i \rightarrow 3/2^-$ and $J_i \rightarrow 1/2^-$ transitions, in the experimental γ spectrum. The exper-

imental γ spectrum has been well reproduced using the Monte-Carlo simulation based on the FRESKO calculation and is presented in Figure 5. This assures the validity of couplings considered for the calculation of discrete components of the direct capture in ${}^6\text{Li}(n,\gamma)$ reaction.

Talys-1.95 calculated continuum component of Direct Capture, Houser-Feshback + Pre-equilibrium components are much lesser compared to the discrete component of the direct capture. Talys calculated discrete component of Direct Capture in ${}^6\text{Li}(n,\gamma)$ is also well in agreement with the experimental cross sections and FRESKO calculations. The inhibition of the compound nuclear component in ${}^6\text{Li}(n,\gamma)$ reaction is due to the lesser number of levels available in the ${}^7\text{Li}$ compound nucleus. Further the strong coupling of $\alpha + t$ breakup is also reducing the capture cross section significantly. The contributions of E1, M1 and E2 mode of γ transitions to the total direct capture are presented in Figure 7. Compared to the E1 mode of transition, the M1 and E2 transition yields are much lower and not contributing significantly to the total radiative capture. The sum of Direct Capture, Houser-Feshback and Pre-equilibrium is well reproducing the experimental cross sections for ${}^6\text{Li}(n,\gamma)$. The Direct Capture, Houser-Feshback and Pre-equilibrium components of neutron capture along with experimental cross sections are illustrated in Figure. 6.

Excitation functions available with ENDF/B-VIII.0, JEEF-3.2 and JENDL-5 are compared with the experimental cross sections and theoretical predictions. The comparison is presented in Figure 4. ENDF/B-VIII.0 and JEEF-3.2 cross sections are identical and not reproducing the theoretical or experimental cross sections above 0.1 MeV. At lower energies, below 0.1 MeV, all the evaluations are matching with the discrete component of the direct capture. But at energies above 0.1 MeV, there is a huge discrepancy between ENDF/B-VIII.0, JEEF-3.2 and JENDL-5. The JENDL-5 is highly over predicts the experimental data. Further, the shape of the excitation function differ significantly from the measured and calculated curves. ${}^6\text{Li}(n,\gamma)$ evaluated data in ENDF/B are obtained by fitting the R-Matrix on the ${}^6\text{Li}(n,\alpha)$, the breakup channel. Hence it is anticipated as this fitting may be inappropriate for accurate parametrisation of the direct capture.

Summarizing, the ${}^6\text{Li}(n,\gamma)$ cross sections ave been deduced by measuring the γ transition probability experimentally and by accounting for the spin factor by theoretical calculation. The initial neutron capture states have been populated through the inelastic scattering of protons in ${}^7\text{Li}$. The method is analogous to the established Oslo method used to measure the neutron capture. However, this current measurement is fulfilled with a single LaBr_3 scintillator, than the total absorption spectrometers (γ calorimeters). This is because of the average multiplicity of the γ events from J_i states covered in this study, are near to unity and the primary γ events were well resolved. The accessibility of this method to the direct capture mechanism is assured by

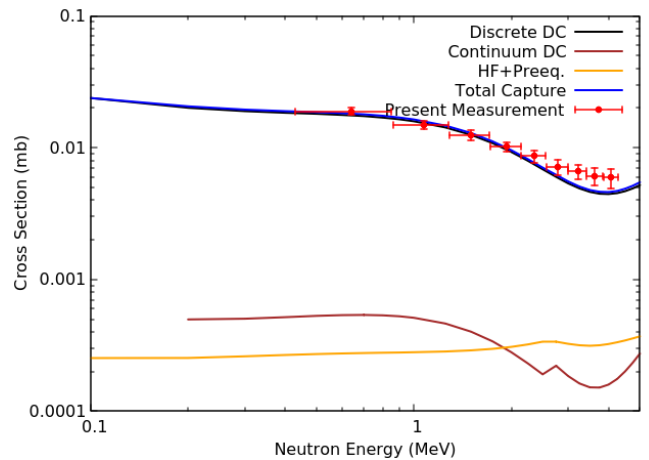


FIG. 6. Discrete and Continuum components of direct capture and the Hauser-Feshbach- + pre-equilibrium component (HF+Preeq) with the the total cross section compared with the experimental data

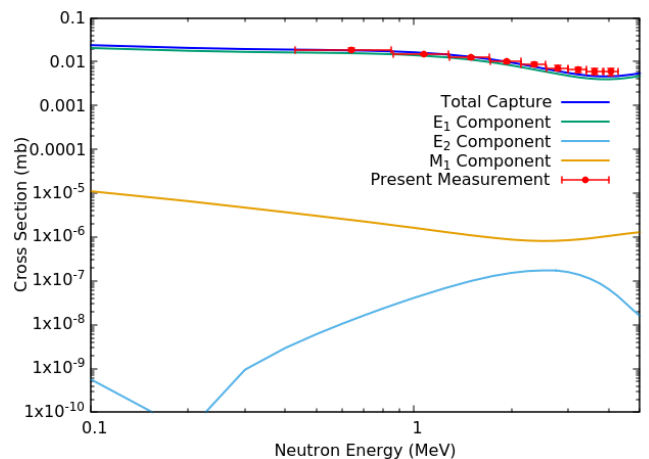


FIG. 7. Contribution of E₁, E₂ and M₁ modes of electromagnetic transition to the total capture cross section.

comparing the measured γ spectrum to the calculated γ spectrum. This shows that the major mechanism involved in ${}^6\text{Li}(n,\gamma)$ is the discrete component of Direct Capture with E1 mode of transition. Continuum component of Direct Capture and HF+Prequilibrium are significantly smaller compared to the discrete component. E2 and M1 components are significantly lesser compared to the E1 mode of transition. The calculations indicate there exist a significant coupling of the $5/2^-$, $7/2^-$ and $3/2^-$ levels, above neutron separation threshold of ${}^7\text{Li}$, to the $J_i \rightarrow 3/2^-$ and $J_i \rightarrow 1/2^-$ transitions in ${}^6\text{Li}(n,\gamma)$ reaction.

ACKNOWLEDGEMENTS

The support of BARC-TIFR Pelletron-LINAC group during the experiment is acknowledged. The authors acknowledge the staff in TIFR Target Laboratory in the

development of Li target for the experiment. The authors acknowledge A. Shanbhag, Health Physics Division, BARC for their kind support during the experiment. This study is part of the project supported by DAE-BRNS, Sanction Order 36(6)/14/30/2017-BRNS/36204.

-
- [1] S. Jun, L. Zhi-Hong, G. Bing, B. Xi-Xiang, L. Zhi-Chang, L. Jian-Cheng, W. You-Bao, L. Gang, Z. Sheng, W. Bao-Xiang, Y. Sheng-Quan, L. Yun-Ju, L. Er-Tao, F. Qi-Wen, and L. Wei-Ping, Neutron spectroscopic factors of ${}^7\text{Li}$ and astrophysical ${}^6\text{Li}(n,\gamma){}^7\text{Li}$ reaction rates, *Chinese Physics Letters* **27**, 052101 (2010).
- [2] C. Aguilera-Gómez, J. Chanamé, and M. H. Pinsonneault, On lithium-6 as a diagnostic of the lithium-enrichment mechanism in red giants, *The Astrophysical Journal* **897**, L20 (2020).
- [3] E. Casuso and J. E. Beckman, On the Origin of the Dispersion in the ${}^7\text{Li}/{}^6\text{Li}$ Ratio in the ISM, *Publications of the Astronomical Society of Japan* **55**, 247 (2003), <https://academic.oup.com/pasj/article-pdf/55/1/247/4321608/pasj55-0247.pdf>.
- [4] R. A. Malaney and W. A. Fowler, On Nuclear Reactions and ${}^9\text{Be}$ Production in Inhomogeneous Cosmologies, *apjl* **345**, L5 (1989).
- [5] K. M. Nollett, M. Lemoine, and D. N. Schramm, Nuclear reaction rates and primordial ${}^6\text{Li}$, *Phys. Rev. C* **56**, 1144 (1997).
- [6] T. Giegerich, K. Battes, J. Schwenzer, and C. Day, Development of a viable route for lithium-6 supply of demo and future fusion power plants, *Fusion Engineering and Design* **149**, 111339 (2019).
- [7] D. Steiner and M. Tobias, Cross-section sensitivity of tritium breeding in a fusion reactor blanket: effects of uncertainties in cross-sections of ${}^6\text{Li}$, ${}^7\text{Li}$, and ${}^{93}\text{Nb}$, *Nuclear Fusion* **14**, 002 (1974).
- [8] Y. Xu and S. Goriely, Systematic study of direct neutron capture, *Phys. Rev. C* **86**, 045801 (2012).
- [9] Y. Xu, S. Goriely, A. J. Koning, and S. Hilaire, Systematic study of neutron capture including the compound, pre-equilibrium, and direct mechanisms, *Phys. Rev. C* **90**, 024604 (2014).
- [10] T. Ohsaki, K. Takaoka, Y. Nagai, H. Kitazawa, and M. Igashira, First measurement of neutron capture cross section of ${}^6\text{Li}$ at stellar energy, *AIP Conference Proceedings* **529**, 678 (2000), <https://aip.scitation.org/doi/pdf/10.1063/1.1361451>.
- [11] N. Otuka et al., Towards a more complete and accurate experimental nuclear reaction data library (exfor): International collaboration between nuclear reaction data centres (nrdc), *Nuclear Data Sheets* **120**, 272 (2014).
- [12] R. B. Firestone and Z. Revay, Thermal neutron radiative cross sections for ${}^6,7\text{Li}$, ${}^9\text{Be}$, ${}^{10,11}\text{B}$, ${}^{12,13}\text{C}$, and ${}^{14,15}\text{N}$, *Phys. Rev. C* **93**, 054306 (2016).
- [13] C. S. Park, G. M. Sun, and H. Choi, Determination of thermal neutron radiative capture cross section of ${}^6\text{Li}$, *Nuclear Instruments and Methods in Physics Research Section B: Beam Interactions with Materials and Atoms* **245**, 367 (2006).
- [14] G. A. Bartholomew and P. J. Campion, Neutron capture gamma rays from lithium, boron, and nitrogen, *Canadian Journal of Physics* **35**, 1347 (1957), <https://doi.org/10.1139/p57-147>.
- [15] D.A. Brown and et al., ENDF/B-VIII.0: The 8th major release of the nuclear reaction data library with cielo-project cross sections, new standards and thermal scattering data, *Nuclear Data Sheets* **148**, 1 (2018), special Issue on Nuclear Reaction Data.
- [16] A. J. M. Plompen et al., The joint evaluated fission and fusion nuclear data library, jeff-3.3, *The European Physical Journal A* **56**, 10.1140/epja/s10050-020-00141-9 (2020).
- [17] K. SHIBATA, O. IWAMOTO, T. NAKAGAWA, N. IWAMOTO, A. ICHIHARA, S. KUNIEDA, S. CHIBA, K. FURUTAKA, N. OTUKA, T. OHSAWA, T. MURATA, H. MATSUNOBU, A. ZUKERAN, S. KAMADA, and J. ichi KATAKURA, Jendl-4.0: A new library for nuclear science and engineering, *Journal of Nuclear Science and Technology* **48**, 1 (2011), <https://doi.org/10.1080/18811248.2011.9711675>.
- [18] M. Guttormsen, T. Tveter, L. Bergholt, F. Ingebretsen, and J. Rekstad, The unfolding of continuum γ -ray spectra, *Nuclear Instruments and Methods in Physics Research Section A: Accelerators, Spectrometers, Detectors and Associated Equipment* **374**, 371 (1996).
- [19] A. Schiller, L. Bergholt, M. Guttormsen, E. Melby, J. Rekstad, and S. Siem, Extraction of level density and γ strength function from primary γ spectra, *Nuclear Instruments and Methods in Physics Research Section A: Accelerators, Spectrometers, Detectors and Associated Equipment* **447**, 498 (2000).
- [20] C. Midhun, M. Musthafa, A. Joseph, J. K.C, and S. Ganesan, Extraction of neutron pulses from coincidence summed events via machine learning - like algorithm, *Proceedings of the DAE International Symp. on Nucl. Phys.* **63**, 1134 (2018).
- [21] S. Agostinelli, Geant4—a simulation toolkit, *Nuclear Instruments and Methods in Physics Research Section A: Accelerators, Spectrometers, Detectors and Associated Equipment* **506**, 250 (2003).
- [22] S. Chiba, K. Togasaki, M. Ibaraki, M. Baba, S. Matsuyama, N. Hirakawa, K. Shibata, O. Iwamoto, A. J. Koning, G. M. Hale, and M. B. Chadwick, Measurement and theoretical analysis of neutron elastic scattering and inelastic reactions leading to a three-body final state for ${}^6\text{Li}$ at 10 to 20 mev, *Phys. Rev. C* **58**, 2205 (1998).
- [23] I. J. Thompson, Coupled reaction channels calculations in nuclear physics, *Computer Physics Reports* **7**, 167 (1988).
- [24] S. Cohen and D. Kurath, Spectroscopic factors for the $1p$ shell, *Nuclear Physics A* **101**, 1 (1967).
- [25] A. Koning, S. Hilaire, and M. Duijvestijn, Talys-1.95, a nuclear reaction program, NRG-1755 ZG Petten, The Netherlands (2019).

- [26] S. Hilaire, M. Girod, S. Goriely, and A. J. Koning, Temperature-dependent combinatorial level densities with the d1m gogny force, *Phys. Rev. C* **86**, 064317 (2012).